A 40-GHz Colliding Pulse Mode-Locked Semiconductor Laser *

Song-Tao Liu(刘松涛)**, Rui-Kang Zhang(张瑞康), Dan Lu(陆丹),
Qiang Kan(阚强), Wei Wang(王圩), Chen Ji(吉晨)

Key Laboratory of Semiconductor Materials Science, Institute of Semiconductors, and Beijing Key Laboratory of Low Dimensional Semiconductor Materials and Devices, Chinese Academy of Sciences, Beijing 100083

(Received 16 February 2016)

A monolithically active–passive integrated colliding pulse mode-locked semiconductor laser is demonstrated in the InGaAsP/InP material system. The device is mode locked at the second harmonic passive mode-locking regime with a wide mode-locking range. Pulse trains with the repetition rate of 40 GHz, 3-dB rf line width of 25 kHz, the pulse width of 2.5 ps, and a nearly transform-limited time–bandwidth product of 0.53 are obtained.

PACS: 42.55.Px, 42.60.Fc, 42.65.Re DOI: 10.1088/0256-307X/33/6/064205

Ultrafast and ultrashort pulse generation from monolithically mode-locked semiconductor lasers are of great interest for future high-speed optical communication applications including high bit rate time-division multiplexed optical networks, optical clock recovery, high-speed optical signal processing, and photonic-assisted analogue-to-digital conversion due to their small footprint, robustness, stability, and potential for massive production.[1–4] Compared with traditional Fabry–Perot two-section type mode-locked configurations, of which typical schemes incorporate a gain section and a saturable absorber (SA) that is integrated on a single substrate sharing the same multiple quantum well active region,[5–8] colliding pulse mode-locked (CPM) lasers place the SA section at the center of the laser cavity, taking advantage of the collision of two counter-propagating pulses in the SA section, which results in an absorption grating, leading to an enhancement of the saturable absorption and therefore more effective pulse shortening.[9–12] CPM lasers with 40-GHz repetition rate have been realized earlier in bulk[13] and multi-quantum well InGaAsP lasers[14] with picosecond pulses obtained. However, both the structures employed an all-active configuration, which would introduce potentially too much quantum noise resulting from amplified spontaneous emission (ASE) of the gain section,[15] leading to broad rf 3-dB line widths of several hundreds of kilohertz, deteriorating the device performance in pragmatic applications. One way to handle this problem is to decrease the optical confinement factor[16,17] that minimizes the amount of coupled ASE noise to the optical mode. The other is to use the active–passive integration technology,[12] where passive sections are introduced to obtain the same mode-locking frequency with minimum length of gain section. Moreover, further integration with other passive waveguide components such as arrayed waveguide grating could be achieved[18] to realize complex functionalities.

In this Letter, we report the fabrication and detailed characterization of a monolithically active–passive integrated 40-GHz CPM laser based on an InGaAsP/InP material system, emitting at ∼1.54 μm. The laser operates in the second harmonic mode-locking regime with a repetition frequency of 40 GHz. Due to the employment of the passive waveguide section, quantum noise resulting from background ASE noise is relatively reduced, leading to a 3-dB rf line width as narrow as 25 kHz. A Gaussian-fit pulse width of 2.5 ps with a nearly transform-limited time–bandwidth product (TBP) of 0.53 is demonstrated.

Figure 1 shows the schematic diagram of the designed CPM laser. The total length of the laser is chosen to be 2060 μm, which consists of two 500-μm-long gain sections, a 70-μm-long SA section, and the rest are passive waveguide sections, with ridge waveguide width of 3.5 μm. The SA is located at the center of the cavity, enabling the second harmonic mode-locking of the laser with a repetition frequency of 40 GHz defined by $f = c/n_{\rm g}L$, where c, $n_{\rm g}$ and L denote the speed of light in free space, the effective group index, and the cavity linear length, respectively. The two gain sections are electrically connected for ease of testing.

The epitaxial structure of the CPM laser was grown on a sulphur-doped InP substrate employing low pressure metal organic chemical vapor deposition (MOCVD). A 0.5-μm-thick n-type InP buffer layer, followed by an undoped 0.25-μm-thick InGaAsP quaternary waveguide layer of bandgap wavelength of 1.25 μm (1.25Q) and an active layer of InGaAsP-based multi-quantum wells (MQWs) was first grown, covering the entire wafer. A SiO_2 mask layer deposited by plasma enhanced chemical vapor deposition (PECVD) was then patterned above the MQWs to form the active region, whereas an unmasked MQWs region was etched away by selective chemical etch to form the passive region. After removing the SiO_2 pattern layer, an undoped upper 1.25Q waveguiding layer (0.25-μm-thick), p-type InP cladding, and the p-type InGaAs contact layer were completed by a single regrowth step

*Supported by the National Natural Science Foundation of China under Grant Nos 61335009, 61274046 and 61474111.
**Corresponding author. Email: stliu@semi.ac.cn
© 2016 Chinese Physical Society and IOP Publishing Ltd

across the entire wafer. A 3.5-μm-wide ridge waveguide formation was then completed by the inductively coupled plasma etching technology. Subsequent wafer backside lapping, p- and n-type metallization, and rapid-thermal-annealing were all followed with standard semiconductor fabrication process. About 7-kΩ electrical isolation was realized by wet etching removal of the heavily doped p-InGaAs contact layer in the 20-μm gap between the gain section and the SA section.

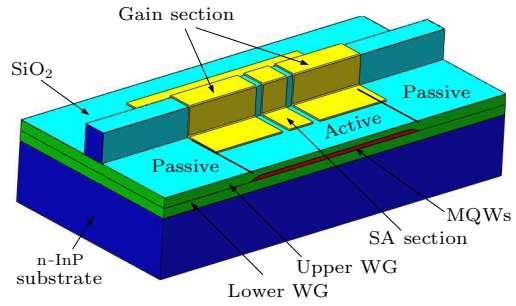

Fig. 1. Schematic diagram of the designed 40-GHz colliding pulse mode-locked laser (WG: waveguide, MQW: multi-quantum well, SA: saturable absorber).

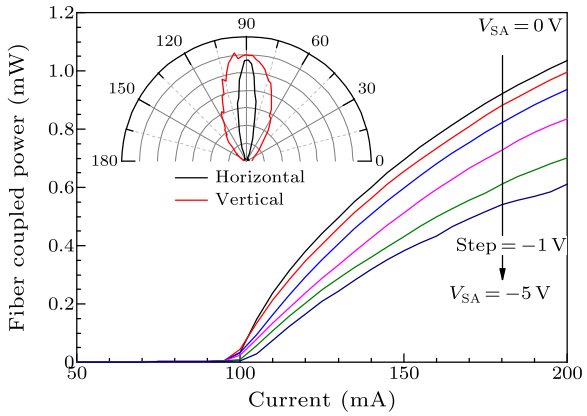

Fig. 2. The cw L–I curves of the CPM device with various bias voltages from 0 V to −5 V with a step of −1 V applied on the 70-μm-long SA section (inset: normalized far-field pattern of the CPM laser with $I_{gain} = 200$ mA and $V_{SA} = 0$ V).

The fabricated 40-GHz CPM laser chips were soldered on Cu heatsinks with both facets left uncoated, and are tested with a thermoelectric cooler (TEC) setting the stage temperature fixed at 10°C. Figure 2 shows the typical light–current (L–I) characteristics of the device with a 70-μm-long SA section. Lasing thresholds vary from 96 mA to 102 mA when the reverse bias of the SA section varies from 0 V to −5 V with steps of −1 V. The slope efficiency decreases with the increase of the reverse biased voltage of the SA section, which is caused by the strengthened quantum-confined Stark effect associated with the increase of the reverse biased voltage that leads to an enhancement in the band-to-band and excitonic absorption[17] of the optical light pulse oscillating in the laser cavity. The normalized far-field pattern of the CPM laser with gain section current of 200 mA and SA reverse voltage of 0 V was also measured and plotted in the inset of Fig. 2, where divergence angles for the horizontal and vertical direction were 20.0° and 53.7°, respectively.

Harmonically passive mode-locking was achieved by properly adjusting the forward biased gain section current and the reverse biased SA section voltage. It was fully characterized by coupling the output of the device to a lensed fiber with a 45 dB optical isolator following and then amplified by an erbium-doped fiber amplifier (EDFA) before routing to an optical spectrum analyzer for spectrum analyzing, a second-harmonic generation (SHG) autocorrelator for time domain analysis, and a signal analyzer with a 50-GHz photodiode for microwave spectrum measurement, respectively.

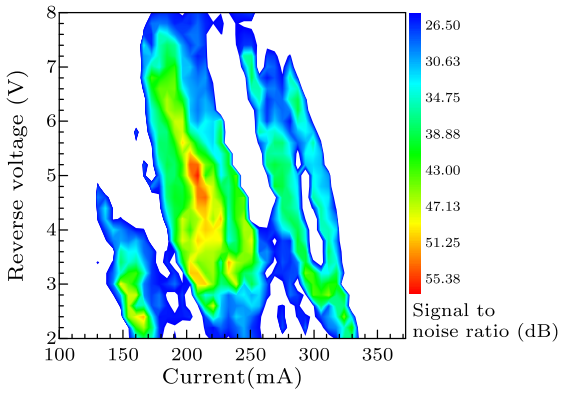

Fig. 3. The intensity of the rf peak over the noise floor at the second harmonic mode-locking frequency as functions of the SOA forward biased current and the SA reverse biased voltage. Only rf signals with the signal-to-noise ratio larger than 25 dB are plotted.

A wide harmonic mode-locking regime of the CPM laser between the SA reverse biased voltage ranging from 2 V to 8 V and the SOA bias current ranging from 125 mA to 325 mA was observed during the characterization, as shown in Fig. 3. The intensity of the rf peak at the second harmonic mode-locking frequency over the noise floor as functions of the gain section current and the absorber reverse voltage is presented, of which proper mode-locking points (signal-to-noise ratio larger than 25 dB[19]) are represented in the color scale. For most of the measured proper mode-locked states the second harmonic frequency peaks in the rf spectrum are higher than 38 dB above the noise floor. Figure 4 shows a detailed characterization of the measured harmonically mode-locked state with the highest signal-to-noise ratio (SNR), where the gain section current and the SA voltage are set at 204 mA and 5.4 V, respectively. The measured spectrum in Fig. 4(a) exhibits mode suppression of every other mode with a side-mode suppression ratio of ∼25 dB in the vicinity of the central mode. The full width at half maximum (FWHM) of the spectrum is about 1.7 nm. Figure 4(b) shows the rf power spectrum over a 50-GHz span. A sharp rf peak can be observed at the second CPM frequency of 40 GHz, of

which the SNR ratio is larger than 55 dB, indicating excellent mode-locking quality. The fundamental frequency was also suppressed perfectly. The measured 3-dB rf spectral linewidth is 25 kHz (see the inset in Fig. 4(b), with the resolution bandwidth (RBW) of 5.1 kHz). The obtained rf linewidth is comparable with those achieved in specially designed mode-locked lasers of AlGaInAs/InP material systems[17] and hybrid silicon mode-locked lasers.[20] The reason for this narrow rf line width can be attributed to the adoption of the active–passive integration scheme, which decreases the length of gain section to reduce the amount of quantum noise arising from background ASE noise coupled to the mode-locked oscillating optical mode.[12,20] Figure 4(c) shows the autocorrelation trace of the pulse measured by using an SHG autocorrelator. The deconvolved pulse width is 2.5 ps assuming a Gaussian pulse shape, which results in a nearly transform-limited TBP value of 0.53 when paired with the spectral width of the optical spectrum. The inset of Fig. 4(c) presents the pulse trains of the measured mode-locked CPM chip, where the pulse interval time is 25 ps, corresponding to a repetition rate of 40 GHz, further confirming the second harmonic mode-locking operation.

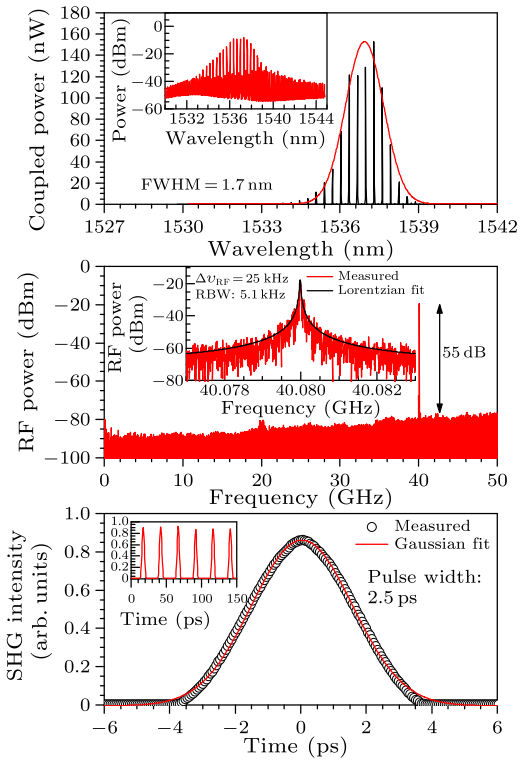

Fig. 4. (a) Optical spectrum in linear and dB (inset) scales and (b) rf spectrum (inset: detailed view of the second harmonic rf peak, RBW=5.1 kHz), and (c) autocorrelation trace of a single isolated pulse (inset: pulse trains in 150-ps span) of the mode-locked CPM laser with $I_{\rm gain}$ = 204 mA, and $V_{\rm SA}$ = 5.4 V, where the highest signal-to-noise ratio is obtained.

Figure 5 shows a typical example of the pulse widths (Fig. 5(a)), 3-dB spectral widths (Fig. 5(b)), and TBP values (Fig. 5(c)) as functions of the gain section forward biased current and the SA section reverse biased voltage of a CPM laser with the same configuration. It can be clearly seen that the pulse widths shorten with the increase of the reverse biased voltage. The FWHMs of autocorrelation traces vary from 2.3 ps to 7.8 ps. The 3-dB spectral widths increase with the increasing reverse bias to a certain point of 6.5 V, which ranges from 0.86 nm to 2.89 nm. Above the point the spectral widths start to reduce as well as the pulse widths begin to increase, which could be attributed to the absorption bands shifting to longer wavelengths due to the high electric field strength applied to the SA section that leads to an absorption mismatch in the spectrum between the gain section and the absorber. The corresponding TBP values vary from 0.47 to 1.21, of which the optimum mode-locking range is from 5.3 V to 6.7 V under the investigated current of 212 mA, where the TBP values are well below 0.5. The reason for larger TBP values outside the optimum mode-locking range is largely due to the self-phase modulation (SPM) effect in both the gain and SA sections.[9]

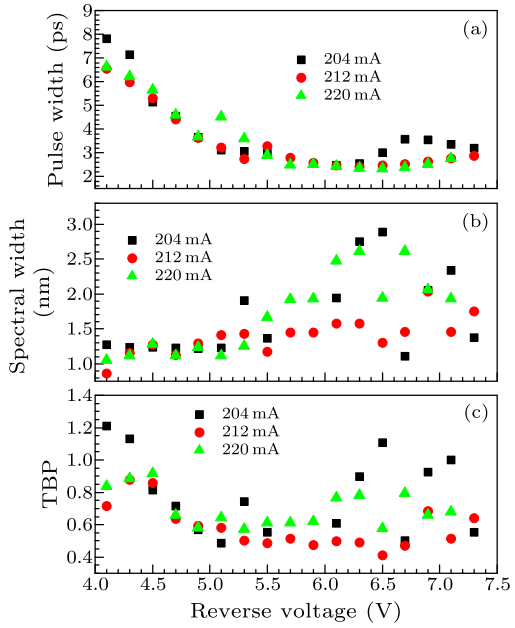

Fig. 5. (a) Pulse widths, (b) 3-dB spectral widths, and (c) time–bandwidth product (TBP) values as functions of the gain section forward biased current and the SA section reverse biased voltage.

In conclusion, we have experimentally investigated a second harmonic colliding pulse mode-locked semiconductor laser fabricated by employing the active–passive integration scheme in an InP material system. The CPM laser is mode-locked for a wide range of the gain under SA section bias conditions. Typical changes of pulse widths, 3-dB spectral widths, and the corresponding TBP values as functions of the gain section forward biased current and the absorber section reversed biased voltage of the same kind of laser are

characterized in detail. The operating frequency of 40 GHz, pulse width of 2.5 ps with a nearly transform-limited TBP value of 0.53 under $I_{\rm gain} = 204$ mA, and $V_{\rm SA} = 5.4$ V of the mode-locked CPM laser chip are demonstrated. The device exhibits excellent mode-locking stability with an SNR over 55 dB and a 3-dB rf spectral line width of 25 kHz, which makes the laser attractive for many future optical applications.

References

[1] Williams K A, Thompson M G and White I H 2004 *New J. Phys.* **6** 179
[2] Bandelow U, Radziunas M, Vladimirov A, Hüttl B and Kailer R 2006 *Opt. Quantum Electron.* **38** 495
[3] Avrutin E A, Marsh J H and Portnoi E L 2000 *IEE Proc.-Optoelectron.* **147** 251
[4] Hou L, Haji M and Marsh J H 2014 *Laser Phys. Lett.* **11** 115804
[5] Du R, Xiang W and Zhang G 2004 *Chin. Opt. Lett.* **2** 36
[6] Kong D, Zhu H, Liang S, Qiu J and Zhao L 2012 *Chin. Phys. Lett.* **29** 024201
[7] Hou L, Stolarz P, Javaloyes J, Green R P, Ironside C N, Sorel M and Bryce A C 2009 *IEEE Photon. Technol. Lett.* **21** 1731
[8] Li M, Ni H, Ding Y, Bajek D, Kong L, Cataluna A and Niu Z 2014 *Chin. Phys.* B **23** 027803
[9] Derickson D J, Helkey R J, Mar A, Karin J R, Wasserbauer J G and Bowers J E 1992 *IEEE J. Quantum Electron.* **28** 2186
[10] Chen Y and Wu M C 1992 *IEEE J. Quantum Electron.* **28** 2176
[11] Thompson M G, Marinelli C, Zhao X, Sellin R L, Penty R V, White I H, Kaiander I N, Bimberg D, Kang D J and Blamire M G 2005 *Electron. Lett.* **41** 248
[12] Ji C, Chubun N, Broeke R G, Cao J, Du Y, Yoo S J B, Liou K Y, Lothian J R, Vatanapradit S, Chu S N G, Patel B, Hobson W S and Tsang W T 2006 *IEEE Photon. Technol. Lett.* **18** 625
[13] Barbarin Y, Bente E A J M, Heck M J R, Oei Y S, Notzel R and Smit M K 2005 *ECOC 31st European Conference on Opt. Communication* **3** 673
[14] Lee H K, Loyo-Maldonado V, Qiu B C, Lee K L, Shu C, Pinches S, Thayne I G, Bryce A C and Marsh J H 2002 *IEEE Photon. Technol. Lett.* **14** 1049
[15] Henry C 1986 *J. Lightwave Technol.* **4** 298
[16] Gee S, Quinlan F, Ozharar S, Delfyett P J, Plant J J and Juodawlkis P W 2005 *Opt. Lett.* **30** 2742
[17] Hou L, Haji M, Akbar J, Qiu B and Bryce A C 2011 *Opt. Lett.* **36** 966
[18] Fontaine N K, Baek J, Ji C, Broeke R, Zhou X, Seo S, Soares F M, Shearn M, Scherer A, Olsson F, Lourdudoss S, Liu K Y, Tsang W T and Yoo S J B 2008 *Opt. Fiber Communication/Natl. Fiber Optic Eng. Conf.* p 1
[19] Barbarin Y, Bente E A J M, Heck M J R, Oei Y S, Nötzel R and Smit M K 2006 *Opt. Express* **14** 9716
[20] Srinivasan S, Davenport M, Heck M J R, Hutchinson J, Norberg E, Fish G and Bowers J E 2014 *Front. Optoelectron.* **7** 265